Unified fluid model analysis and benchmark study for electron transport in gas and liquid analogs

2017 Plasma Sources Sci. Technol. 26 075003

(http://iopscience.iop.org/0963-0252/26/7/075003)

IOP Publishing Plasma Sources Science and Technology
Plasma Sources Sci. Technol. **26** (2017) 075003 (16pp) https://doi.org/10.1088/1361-6595/aa73c6

Unified fluid model analysis and benchmark study for electron transport in gas and liquid analogs

N A Garland[1], D G Cocks[1], G J Boyle[1], S Dujko[2] and R D White[1]

[1] College of Science & Engineering, James Cook University, Townsville, QLD 4810, Australia
[2] Institute of Physics, University of Belgrade, PO Box 68, 11080 Zemun, Belgrade, Serbia

E-mail: nathan.garland@my.jcu.edu.au

Received 23 March 2017, revised 5 May 2017
Accepted for publication 17 May 2017
Published 14 June 2017

Abstract

The interaction of plasmas with liquids requires an understanding of charged particle transport in both the gaseous and liquid phases. In this study we present a generalized fluid-equation framework to describe bulk electron transport in both gaseous and non-polar liquid environments under non-hydrodynamic non-equilibrium conditions. The framework includes liquid structural effects through appropriate inclusion of coherent scattering effects and adaption of swarm data to account for the modification to the scattering environment present in such systems. In the limit of low-densities it reduces to the traditional gas-phase fluid-equation model. Using a higher-order fluid model (four moments), it is shown that by applying steady state electron swarm data in both the gaseous and liquid phases, to close the system of equations and evaluate collisional rates, an improvement in macroscopic electron transport results over popular existing assumptions used. The failure of the local mean energy approximation in fluid models to accurately describe complex spatial oscillatory structures in both the gaseous and liquid phases is discussed in terms of the spatial variation of the electron distribution function itself.

Keywords: fluid modeling, coherent scattering, gas and liquid discharges, low temperature plasma, fluid model closure, non-local transport

1. Introduction

In recent years there has been much interest across multiple research disciplines in investigating the interaction of gas phase plasmas with liquids, culminating in the recent plasma–liquid interactions roadmap [1]. Many research areas in environmental science, materials science, particle detector physics, plasma medicine, and electrical switching necessitate a good understanding of the gas–liquid interface [1–3]. In particular, one point of focus identified in the plasma–liquid interactions roadmap was *charged species transfer across the gas–liquid interface including electron-induced reactions and energy transfer* [1]. The primary objective of this study is to provide a benchmarked platform for modeling electron transport in plasma–liquid interfaces in future studies. To accomplish this, we present the formulation, benchmarking, and analysis of a unified fluid model applied to electron transport in a dilute gas and non-polar simple liquid.

Modeling of charged particle transport in non-equilibrium gas discharges has been studied for some decades. From two-term and multi-term solutions of Boltzmann's equation or particle-in-cell (PIC) and Monte Carlo (MC) methods [4–8], giving accurate microscopic descriptions, through to computationally simpler fluid methods [9–16], providing macroscopic, qualitative descriptions of discharge dynamics, there are many options available for modeling a gas phase discharge.

Despite the advantages in simplicity and computational benefits, approximations are necessary to describe the functional dependence of input data for fluid modeling. Much work has been done using the classic local field approximation (LFA) [9, 12, 17] describing reduced electric field, $\frac{E}{n_0}$, dependent mobility and diffusion coefficients, and collision rates. While the local energy approximation (LEA) has also been used to attempt to describe non-local dependence through mean energy dependent transport coefficients and rates [10, 12, 14–16, 18, 19].

In addition to these approximations, closure assumptions must be made to truncate the infinite series of moment equations [12, 20]. Traditionally, drift-diffusion approximations (DDAs) in the steady-state limit have been used, with approximations often made on the electron heat flux [10, 12, 14, 17, 18]. Neglecting the heat flux or using a Fourier law type assumption are common approaches in existing literature [10, 12]. Additionally, a parameterized, steady state ansatz has been proposed to capture periodic electron structures in gases [12, 21, 22]. In recent times four moment models have been used to defer closure to a higher order moment equation, with parameterized ansatz and steady-state input closure methods being proposed and applied in recent studies [14–16, 18, 20].

In comparison to gas phase modeling, liquid discharges add many complications, such as structure effects, electron solvation, and evaporation, which make a complete modeling approach difficult [1–3, 23–25]. Recent modeling studies have used electric conductivity and permittivity changes between model material phases [2], directly modified gas phase electron diffusion coefficients [24, 25], or constant empirical transport coefficients and rates [3, 25] all to good effect in order to provide new understanding of gas–liquid interfaces.

Motivated by these efforts we seek to extend a recent kinetic formulation [23, 26, 27], which introduced a structure factor modification to account for coherent scattering effects in dense media. Ultimately we seek to formulate and benchmark a generalized electron fluid model that will later be applied to modeling electron transport between a plasma–liquid interface, where liquid processes, such as solvation, may be included at a fundamental level via electron collision cross sections [23].

The formulation of the fluid model for both gas and simple liquids with coherent scattering effects is presented in section 2. A parameter-free, unified steady state closure assumption is introduced, along with a brief summary of existing closure approaches commonly used in fluid modeling. Steady state and transient benchmarking of the electron fluid model against accurate MC simulations and multi-term solutions of the Boltzmann equation are presented in section 3 to demonstrate the utility of the fluid model. From this benchmarking, comparisons of results from the alternative fluid models presented in section 2 are shown in order to highlight significant differences that can occur in various benchmark scenarios. Finally, a brief discussion of the impact of variation in electron energy distribution functions is included to rationalize the limitations of the local mean energy approximation. Concluding remarks are detailed in section 4.

2. Theory

2.1. Fluid modeling

The microscopic dynamics of charged particle transport in gases or liquids alike can be described by particle-based simulations or directly solving the Boltzmann equation of kinetic theory [28, 29]

$$\frac{\partial f}{\partial t} + \mathbf{v}\cdot\frac{\partial f}{\partial \mathbf{r}} + \mathbf{a}\cdot\frac{\partial f}{\partial \mathbf{v}} = -J(f), \tag{1}$$

which describes the evolution of the charged particle ensemble distribution function $f(\mathbf{r}, \mathbf{v}, t)$ in position-velocity phase space $(\mathbf{r}, \mathbf{v})$ [4, 5, 8, 30], where $\mathbf{a}$ is an acceleration vector due to applied field (e.g. electric, magnetic, gravitational). The right-hand side of (1) denotes the rate of change of $f(\mathbf{r}, \mathbf{v}, t)$ due to collisions of charged particles with neutral background particles in a gas or soft condensed medium through the collision operator

$$J(f) = J_{\text{coherent}} + J_{\text{incoherent}} = J_{\text{elas}} + J_{\text{inel}} + \ldots \tag{2}$$

which describes all possible scattering processes, such as elastic collisions, inelastic collisions, attachment, and ionization, through appropriate cross-sections. An important distinction between coherent (i.e. elastic) and incoherent scattering processes needs to be made for the consideration of charged particle transport in liquid and soft-condensed structured systems [23].

PIC or MC are the leading particle-based methods used to simulate charged particle distributions in phase space [7, 15], while two-term [6] or modern multi-term solutions [23, 27] of the Boltzmann equation are the leading methods that solve directly for the particle distribution.

Microscopic kinetic approaches provide very accurate descriptions of charged particle transport but become mathematically complicated and computationally time consuming for applications containing complex geometries or boundaries, multiple spatial dimensions, or many charged species. Applications involving plasma–liquid interfaces typical contain these complications, and so a simpler, computationally efficient modeling approach is sought. As such, the modeling approach chosen in this study is a fluid or moment model [9, 10, 12, 16, 18, 31, 32].

Fluid models provide a description of a swarm or plasma through velocity-averaged variables. This gives a macroscopic model of the discharge, which retains only the direct quantities important for evolution of the system. This approach gives a significant boost to calculation speed, while maintaining reasonable accuracy of quantities of interest. The simplest of these variables is the number density of a species, defined as

$$n(\mathbf{r}, t) = \int f(\mathbf{r}, \mathbf{v}, t)\mathrm{d}\mathbf{v}, \tag{3}$$

while general velocity-averaged quantities are defined from the distribution function

$$\langle \Phi_k \rangle(\mathbf{r}, t) = \frac{1}{n(\mathbf{r}, t)} \int f(\mathbf{r}, \mathbf{v}, t)\Phi_k(\mathbf{v})\mathrm{d}\mathbf{v}, \tag{4}$$

where $\Phi_k(\mathbf{v})$ is any velocity dependent function, and $\langle \ldots \rangle$ denotes the expectation value, a velocity average over $f(\mathbf{r}, \mathbf{v}, t)$.

Generally the moments of trial functions $\Phi_1 = 1$, $\Phi_2 = \mathbf{v}$, $\Phi_3 = \frac{1}{2}mv^2$, $\Phi_4 = \frac{1}{2}mv^2\mathbf{v}$ are performed to get balances on electron number, particle flux, energy density, and energy density flux respectively.

The generic moment equation may be derived by multiplying the Boltzmann equation (1) by an arbitrary, velocity dependent, trial function $\Phi(\mathbf{v})$ and integrating over velocity space [12, 18]

$$\frac{\partial}{\partial t}(n\langle\Phi\rangle) + \nabla\cdot(n\langle\mathbf{v}\Phi\rangle) - n\mathbf{a}\cdot\langle\nabla_{\mathbf{v}}\Phi\rangle = C_{\Phi}, \tag{5}$$

where C_{Φ} is the rate of change of the quantity Φ due to collisions

$$C_{\Phi} = \left(\frac{\partial[n\langle\Phi(\mathbf{v})\rangle]}{\partial t}\right)_{\text{coll}} = -\int\Phi(\mathbf{v})J(f)\mathrm{d}\mathbf{v}. \tag{6}$$

Where this approach departs from classical gas phase fluid models is that the collision term can be written as the sum of coherent and incoherent components

$$C_{\Phi} = C_{\Phi\,\text{coherent}} + C_{\Phi\,\text{incoherent}}. \tag{7}$$

High densities in liquid like states require many modifications to the simple gas phase picture, and including coherent scattering is an attempt to do so. Coherent scattering is projected entirely onto the momentum transfer elastic scattering cross section while inelastic collisions off different molecules are incoherent as they modify the state of the background medium. Assuming, for simplicity, that excitations in a dense medium are localized to individual molecules, incoherent processes are computed by evaluating equation (6) with the semi-classical Boltzmann collision operator [33]. Hence, for all inelastic processes in gas or liquid media, and elastic scattering in dilute gases, the incoherent collision term is found via the traditional collision term

$$C_{\Phi\,\text{incoherent}} = \sum_{j,j'}\int\mathrm{d}\mathbf{v}f(\mathbf{v})\int\mathrm{d}^2\Omega_{\mathbf{g}'}n_0 v\sigma \times(j,j';g,\chi)[\Phi'-\Phi]_{j,j'}, \tag{8}$$

where indices j, j' denote the before and after collision states due to each collisional processes causing internal energy transitions ($\epsilon_j \rightarrow \epsilon_{j'}$) in the neutral particle. Furthermore, g denotes the relative speed between charged particle and neutral scattering center, $\mathrm{d}^2\Omega_{\mathbf{g}'}$ denotes the differential scattering angle $\mathrm{d}\psi\mathrm{d}\chi\sin\chi$ (where ψ is the polar angle and χ the azimuthal angle), and $\sigma(j,j';g,\chi)$ represents the partial cross section for scattering through the azimuthal angle χ given an incoming speed g.

However, when dense mediums or low electron energies are considered, coherent scattering effects are vital. The most general view of charged-particle interactions with a dense medium is the scattering of a wave, representing the charged particle, by the medium as a whole and not a single fixed scattering center. A first approximation to the scattering is the *single-scatterer approximation* [34] in which the scattered wave is the coherent sum of contributions from many scattering centers in the molecule, which interfere to effectively produce a diffraction pattern of the medium [23]. These effects are significant when the electron de Broglie wavelength is comparable to the average background particle spacing, $\lambda\sim\frac{1}{n_0^{\frac{1}{3}}}$.

From the definition of the double differential cross section, the expression for the rate of change of $\Phi(\mathbf{v})$ due to coherent elastic scattering is

$$\frac{\partial}{\partial t}(n\langle\Phi\rangle)\Big|_{\text{coherent}} = \int\mathrm{d}\mathbf{v}f(\mathbf{v})\int_0^{\infty}\mathrm{d}\omega' \times\int_{\hat{\mathbf{k}}'}\mathrm{d}\hat{\mathbf{k}}'n_0 v\frac{\mathrm{d}^2\sigma}{\mathrm{d}\hat{\mathbf{k}}'\mathrm{d}\omega'}[\Phi(\mathbf{v})-\Phi(\mathbf{v}')], \tag{9}$$

where ω' and $\mathbf{k}'$ denote the angular frequency and wavenumber of the charged particle wave after the interaction with the material. The double differential cross section is written as a product of the single atomic differential cross section and the dynamic structure factor [34]

$$\frac{\mathrm{d}^2\sigma}{\mathrm{d}\hat{\mathbf{k}}'\mathrm{d}\omega'} = \sigma_{\text{lab}}\left(|\Delta\mathbf{k}|-\frac{\omega}{2},\hat{\mathbf{k}}'\right)S(\Delta\mathbf{k},\Delta\omega),$$

where $\Delta\mathbf{k}=\mathbf{k}-\mathbf{k}'$ is the change in the wave vector, such that $\mathbf{p}=m\mathbf{v}=\hbar\mathbf{k}$, and $\Delta\omega=\omega-\omega'$ is the change in energy, such that $\epsilon=\hbar\omega=\frac{\hbar^2k^2}{2m}$. Dashed quantities refer to post-collision values. All expressions are evaluated in the laboratory frame in contrast to the single molecule scattering case where collisions are carried out in the center of mass frame, for interactions with many particles simultaneously this is not possible.

Equations (5)–(9) now provide a complete framework for generating charged particle fluid equations in both gas and liquid media alike. In the limit of high incoming particle energies or dilute gases, equation (9) reduces to equation (8) where $S(\Delta\mathbf{k},\Delta\omega)$ has zero contribution from correlations between atoms [23, 27].

2.2. Four moment electron fluid model

For electrons of charge q_e and mass m_e, in a gas or liquid subject to a homogeneous background electric field, $\mathbf{E}$, such that the acceleration vector is

$$\mathbf{a} = \frac{q_e}{m_e}\mathbf{E}, \tag{10}$$

the first four moment equations can be derived from equations (5)–(9) by substituting $\Phi = 1$, $\mathbf{v}$, $\frac{1}{2}mv^2$, $\frac{1}{2}mv^2\mathbf{v}$

$$\frac{\partial n}{\partial t} + \nabla\cdot\mathbf{\Gamma} = n(\nu_I^{\text{ss}}(\langle\epsilon\rangle) - \nu_a^{\text{ss}}(\langle\epsilon\rangle)), \tag{11}$$

$$\frac{\partial\mathbf{\Gamma}}{\partial t} + \nabla\cdot(n\theta_m) - n\frac{q_e}{m_e}\mathbf{E} = -\Gamma\nu_m^{\text{ss}}(\langle\epsilon\rangle), \tag{12}$$

$$\frac{\partial n_\epsilon}{\partial t} + \nabla\cdot\mathbf{\Gamma}_\epsilon - q_e\mathbf{E}\cdot\mathbf{\Gamma} = -nS_\epsilon^{\text{ss}}(\langle\epsilon\rangle), \tag{13}$$

$$\frac{\partial\mathbf{\Gamma}_\epsilon}{\partial t} + \nabla\cdot(n\theta_\xi) - n\theta_m\cdot q_e\mathbf{E} - n_\epsilon\frac{q_e}{m_e}\mathbf{E} = -\Gamma_\epsilon\nu_\xi^{\text{ss}}(\langle\epsilon\rangle), \tag{14}$$

where shorthand variables for particle flux, energy density, and energy density flux are

$$\Gamma = n\langle\mathbf{v}\rangle = \int f(\mathbf{r},\mathbf{v},t)\mathbf{v}\mathrm{d}\mathbf{v}, \tag{15}$$

$$n_\epsilon = n\langle\epsilon\rangle = \int f(\mathbf{r}, \mathbf{v}, t)\frac{1}{2}mv^2 \mathrm{d}\mathbf{v}, \tag{16}$$

$$\Gamma_\epsilon = n\langle\boldsymbol{\xi}\rangle = \int f(\mathbf{r}, \mathbf{v}, t)\frac{1}{2}mv^2\mathbf{v}\mathrm{d}\mathbf{v}, \tag{17}$$

with $\langle\mathbf{v}\rangle$, $\langle\epsilon\rangle$, and $\langle\boldsymbol{\xi}\rangle$ being the electron average velocity, average energy, and average energy flux. Higher order tensor products $\theta_m = \langle\mathbf{vv}\rangle$ and $\theta_\xi = \left\langle\frac{1}{2}mv^2\mathbf{vv}\right\rangle$ are introduced, and require closure approximations in order to numerically solve the system.

Consistent with existing modeling literature [6, 9–11, 13–16] the collision terms are approximated via pre-computing *steady state* expectation values of reduced collision rates, $\left\langle\frac{\nu}{n_0}\right\rangle$, through MC simulations [7, 26] or multi-term solutions of the Boltzmann equation [23, 27] of a steady state distribution function, and interpolating as a function of the local mean energy.

It should be noted that in this work, input rates and closure input to follow have been written as parameter-free expectation values over the steady state distribution function, independent of the computational method such as MC simulation or a multi-term solution of the Boltzmann equation. For a given method there will be simplified expressions written in terms of isotropic and anisotropic distribution function components, f_0, f_1, f_2 and so on. For further details, we refer the reader to previous publications on the MC methods [7, 26] and multi-term kinetic methods [8, 23, 27, 35] used in evaluation of the input data for this study.

Given ionization and attachment cross sections, σ_I and σ_a, expressions for the ionization and attachment rates are

$$\nu_I^{\mathrm{ss}} = \left\langle n_0\sqrt{\frac{2\epsilon}{m_e}}\sigma_I(\epsilon)\right\rangle_{f_{\mathrm{ss}}}, \tag{18}$$

$$\nu_a^{\mathrm{ss}} = \left\langle n_0\sqrt{\frac{2\epsilon}{m_e}}\sigma_a(\epsilon)\right\rangle_{f_{\mathrm{ss}}}, \tag{19}$$

where subscript f_{ss} denotes the expectation value is performed by integration over the steady state distribution function.

The vector quantity collision rates for momentum and energy flux transfer are computed from the steady state distribution function by normalizing the loss-rate of each given quantity to its steady state value,

$$\nu_m^{\mathrm{ss}} = \frac{\langle\Delta\mathbf{v}\nu_T(\epsilon)\rangle_{f_{\mathrm{ss}}}}{\langle\mathbf{v}\rangle_{f_{\mathrm{ss}}}}, \tag{20}$$

$$\nu_\xi^{\mathrm{ss}} = \frac{\langle\Delta\xi\nu_T(\epsilon)\rangle_{f_{\mathrm{ss}}}}{\langle\boldsymbol{\xi}\rangle_{f_{\mathrm{ss}}}}, \tag{21}$$

where $\Delta\mathbf{v}$ and $\Delta\boldsymbol{\xi}$ denote the average change in velocity and energy flux per collision, averaged over all possible processes, and ν_T is the total collision rate in the steady state.

The energy transfer rate S_ϵ is the lump sum of average energy losses due to all collisional processes

$$S_\epsilon^{\mathrm{ss}} = \langle\Delta\epsilon\nu_T(\epsilon)\rangle_{f_{\mathrm{ss}}}, \tag{22}$$

where $\Delta\epsilon$ is the average change of energy per collision averaged all possible processes, including any threshold and collision energy transfer.

2.2.1. Steady state closure. In lieu of assuming analytic forms of velocity distribution functions for closure approximations or parameterizing closure expressions as functions of known moment variables, as often done in the past [12, 31], we prefer utilizing steady state electron distribution functions as recently proposed by Becker and Loffhagen [14, 16, 20, 31, 35] to evaluate closure terms, akin to the collision input terms Motivated by the work in [20] through equations (15*a*)–(15*d*), we utilize MC simulations [7, 26] or multi-term solutions of the steady state electron energy distribution function [23, 27] to generate a look-up table of closure terms

$$\theta_m \approx \theta_m^{\mathrm{ss}}(\langle\epsilon\rangle) = \langle\mathbf{vv}\rangle_{f_{\mathrm{ss}}}, \tag{23}$$

$$\theta_\xi \approx \theta_\xi^{\mathrm{ss}}(\langle\epsilon\rangle) = \left\langle\frac{1}{2}mv^2\mathbf{vv}\right\rangle_{f_{\mathrm{ss}}}, \tag{24}$$

as well as the usual collision rates, as a function of the local electron mean energy. This model will be referred to as '*4MM-SS*' in the remainder of this work.

Using steady state distribution closure ensures that electron transport evolves in a manner guided by a physically motivated distribution function. In regimes that are known to not produce oscillatory structures, due to reduced electric field and collision cross section effects, we believe this fluid model has a higher potential to accurately resolve spatially averaged electron transport quantities, as demonstrated in section 3.

In non-hydrodynamic regimes far from the steady state distribution we acknowledge that detailed electron structures, such as periodic spatial phenomena [21, 22], will be difficult to generally replicate with this steady state closure approach, as shown by a benchmarked analytic steady-state heat flux ansatz [12, 21, 31]. Despite this limitation in the steady-state closure, we believe using a parameter free, general closure assumption offers a flexible option to the fluid modeling community as it is applicable in time-dependent and steady state problems, and requires no tuning of input parameters or benchmarking.

We believe that this closure approximation is sufficient to reproduce the general evolution of space–time electron transport, in a 'line of best fit' sense sufficient for basic studies of discharges in either gaseous or liquid media. To be discussed in section 3.6, we believe the difficulty of fluid models to resolve oscillatory structures lies in their inability to resolve distribution function variations due to the local mean energy approximation, and not in the choice of closure approximations.

2.2.2. Drift-diffusion approximations. Often low-temperature plasma modeling studies will be concerned with long-time scale or steady state simulations [10, 14, 15, 31, 36], and DDAs are commonly employed. As such, we present a simplified version of the previous four moment model into a two moment model consisting of the two continuity equations for number density (11) and energy density (13) but with

steady state particle (25) and energy flux (26) expressions

$$\Gamma^{\rm ss} = \frac{1}{\nu_m^{\rm ss}(\langle\epsilon\rangle)}\left[\frac{q_e}{m_e}n\mathbf{E} - \nabla\cdot(n\theta_m^{\rm ss}(\langle\epsilon\rangle))\right], \tag{25}$$

$$\Gamma_\epsilon^{\rm ss} = \frac{1}{\nu_\xi^{\rm ss}(\langle\epsilon\rangle)}\left[q_e n\theta_m^{\rm ss}(\langle\epsilon\rangle)\cdot\mathbf{E} + \frac{q_e}{m_e}n_\epsilon\mathbf{E} - \nabla\cdot(n\theta_\xi^{\rm ss}(\langle\epsilon\rangle))\right], \tag{26}$$

where collision and closure inputs are the same as prescribed for the four moment model, *4MM-SS*.

This approximate model is justified by assuming the relaxation collision frequencies of the vector quantities is much faster than the time scales for energy relaxation and electron transport, through electric field driven advection or diffusive transport [12, 37]. This model will be referred to as '*DDA-SS*' in the remainder of this work.

2.3. Other fluid models

In order to facilitate comparison of the presented fluid model using steady state closure, three fluid models previously used in literature are briefly presented: parameterized four moment closure, zero heat flux, and a Fourier law heat flux closure.

We note a method of closure through an analytic heat flux ansatz benchmarked against an asymptotic perturbation solution of the balance equations has been proposed [12, 21]. We acknowledge the benefits of this method, but concerns regarding the choices of tunable free parameters in benchmarking new collision models, as well as the fact this ansatz is grounded in the steady state, leads us to prefer more generalized approaches to closure of the balance equations. The anzatz of Nicoletopoulos and Robson [12, 21] should however motivate future work on introducing the effects of energy transfer due to inelastic collisions into the closure of fluid models in order to model complex structures.

2.3.1. Parameterized Four Moment Model. In previous work by Dujko *et al* [15, 18, 38] a four moment fluid model was presented with focus on application to streamer propagation; this model will be referred to as '*4MM-D*' in the remainder of this work. Functionally, this model is identical to the four moment model presented in this study (11)–(14), but with different closure assumptions. Closure of the momentum balance higher order term, θ_m, is achieved by assuming a Maxwellian distribution [12, 18] and isotropic temperature tensor in order to yield the following standard closure expression

$$\theta_m \approx \frac{2}{3m_e}\langle\epsilon\rangle\mathsf{I}, \tag{27}$$

where I is the identity tensor.

Extending this assumption to closing the energy flux balance equation, and assuming the higher order energy flux closure term can be approximated by

$$\theta_\xi \approx \beta\left\langle\frac{1}{2}mv^2\right\rangle\langle\mathbf{vv}\rangle, \tag{28}$$

an ansatz is constructed for second closure term

$$\theta_\xi \approx \beta\frac{2}{3m_e}\langle\epsilon\rangle^2\mathsf{I}, \tag{29}$$

where β is a parameterization factor nominally close to unity [18, 38]. In this study, it was assumed $\beta = 1$ as per the author's original work.

2.3.2. Drift diffusion models. One of the simplest, and most popular, approaches to fluid modeling is a drift diffusion model with hydrodynamic transport coefficients applied to a density gradient expansion [10, 12, 14, 15]. This approach utilizes two continuity equations for number density (11) and energy density (13), with particle and energy density flux expressions closing the system. Traditionally the particle flux is written

$$\Gamma = -n\mu(\langle\epsilon\rangle)\mathbf{E} - \mathsf{D}(\langle\epsilon\rangle)\nabla n, \tag{30}$$

where electron mobility and longitudinal diffusion coefficients, μ and D_L in a 1D model, are tabulated as a function of the local reduced electric field or electron mean energy as per the collision input from previous models. In keeping with recent studies demonstrating non-local effects in gas discharges [10, 12, 19, 22, 39, 40], the local mean energy approximation is used in application of these drift diffusion models in lieu of the LFA.

In contrast to particle flux closure, a number of methods have been previously used to approximate the energy density flux expression [9, 10, 12, 14–16, 18, 21, 36]. The simplest approach is to neglect the heat flux by fixing it to zero [12, 15]; this model will be referred to as '*DDA-Z*' in the remainder of this work. The zero heat flux closure of equation (33) can be derived by expanding the energy density flux $\Gamma_\epsilon = \frac{1}{2}mn\langle v^2\mathbf{v}\rangle$ using the identity

$$\Gamma_\epsilon = n_\epsilon\langle\mathbf{v}\rangle + \mathsf{P}\cdot\langle\mathbf{v}\rangle + \mathbf{J}_q, \tag{31}$$

where P is the pressure tensor, simplified by assuming a Maxwellian energy distribution to yield the common isotropic pressure tensor expression

$$\mathsf{P} \approx \frac{2}{3}n_\epsilon\mathsf{I}. \tag{32}$$

If the heat flux is then assumed very small such that it can be neglected, $\mathbf{J}_q^z = 0$, we can rewrite equation (31) by substituting for the particle flux, $\Gamma = n\langle\mathbf{v}\rangle$,

$$\Gamma_\epsilon = \frac{5}{3}n_\epsilon\langle\mathbf{v}\rangle = \frac{5}{3}\langle\epsilon\rangle\Gamma, \tag{33}$$

where Γ is the particle flux defined in equation (30).

Another common approach to constructing a heat flux ansatz is by assuming a Fourier's law of heat conduction style closure [10, 41]; this model will be referred to as *DDA-F* in the remainder of this work. A Fourier heat flux ansatz may be derived by assuming a Fourier law type relation for the

heat flux

$$\mathbf{J}_q^F = -\frac{5}{3} n \mathsf{D} \nabla \langle \epsilon \rangle, \tag{34}$$

such that the flux of heat transfer is proportional to some conductivity multiplied by the mean energy gradient [10, 41].

Combining equations (31) and (34) and rewriting as a gradient of n_ϵ we obtain

$$\Gamma_\epsilon = -\frac{5}{3} n_\epsilon \mu(\langle \epsilon \rangle) \mathbf{E} - \frac{5}{3} \mathsf{D}(\langle \epsilon \rangle) \nabla n_\epsilon, \tag{35}$$

where μ and D are the electron mean energy dependent electron mobility and diffusion coefficients.

Despite being based on an analytic distribution, the closure expression (35) does allow for energy density spatial gradients to induce energy transfer—an improvement over the zero heat flux assumption. The formulation and further implications of the Fourier law assumption are detailed in [10, 12].

3. Benchmark results and discussion

Benchmarking is a valuable process in evaluating a model and the integrity of numerical solutions. We have chosen simple benchmark cases with a simple collision model for a gas and liquid analog. This was done to allow comparison of the fundamental transport effects of the fluid equations and their approximations, without introducing nuances of real gases that may introduce phenomena specific to that molecule. A one-dimensional steady state field perturbation benchmark problem and a non-hydrodynamic transient evolution benchmark are presented in this work. Benchmarks were performed in both gas phase and an approximated liquid phase through modifications to the gas phase model. The flux corrected transport (FCT) numerical method employed to solve the systems of hyperbolic equations in this study is based on popular methods used for many years [42–44], and is further outlined in the appendix, along with the dimensional scaling of variables used in this work.

3.1. Gas phase collision model

A simple constant cross section inelastic step collision model has been studied in this work, as per table 1. The model was chosen because despite its simplicity, it can produce physically complex results such as periodic electron structures and relaxation behavior [14, 21, 31, 45] observed in real gases used in benchmark computations, such as argon or neon. With the simplicity of implementation, yet complex non-hydrodynamic transport behavior, we believe this collision model provides a good analog gas for benchmarking the performance of fluid models.

3.2. Liquid phase modification

To approximate transport in a simple, non-polar liquid-like medium a structure modification to the gas phase collision model in table 1 was performed within the computation of steady state transport and collision input via kinetic solution or MC simulation of the Boltzmann equation [7, 12, 27, 30]. This was done via including a static structure modification into the momentum transfer cross section, through the Percus–Yevick liquid model with the correction of Verlet and Weiss [26, 46]. The structure of neutral molecules is assumed to consist of an array of hard sphere potentials interacting coherently, with a density governed by a packing factor

Table 1. Constant cross section inelastic step collision model.

Variable	Value
σ_m	6 Å^2
σ_{inel}	0.1 Å^2, $\epsilon \geqslant \Delta\epsilon_{\text{inel}}$
$\Delta\epsilon_{\text{inel}}$	2 eV
m_0	4 amu
m_e	5.486×10^{-4} amu
T_0	0 K

$$\phi = \frac{4}{3} \pi r^3 n_0, \tag{36}$$

where r is the hard sphere radius, and n_0 is the neutral number density.

A packing factor of $\phi = 0$ corresponds to a classic dilute gas, while the maximum value of $\phi \approx 0.64$ corresponds to a maximally packed solid of hard spheres. For the simple liquid approximation in this study a packing factor of $\phi = 0.4$ was used [27]. Further details of this liquid phase modification in the MC simulations or multi-term solution of Boltzmann's equation can be found in the recent work by the JCU group [23, 26, 27].

3.3. Input data

Given the collision model specified in the previous section, a collection of steady state input data was generated via MC simulations. By generating two sets of the necessary steady state input data for fluid models described in this study, one each for gas and liquid analogs, the same fluid model formulations can be used to simulate electron transport, given the basis of the gas phase collision model in table 1 and simple liquid modifications previously outlined.

The inclusion of coherent scattering effects in the liquid phase results in variations of the fluid model input data from the classic dilute gas picture. We present a comparison of the gas and liquid phase transport input data in the following figures.

3.3.1. Hydrodynamic transport coefficients. The variation of the electron reduced mobility, $n_0\mu$, and reduced longitudinal diffusion coefficient, $n_0 D_L$, between gas and liquid phase transport is shown in figures 1(a) and (b) respectively. The increased mobility and diffusion at low energy due to coherent scattering are clearly noted, as well as the

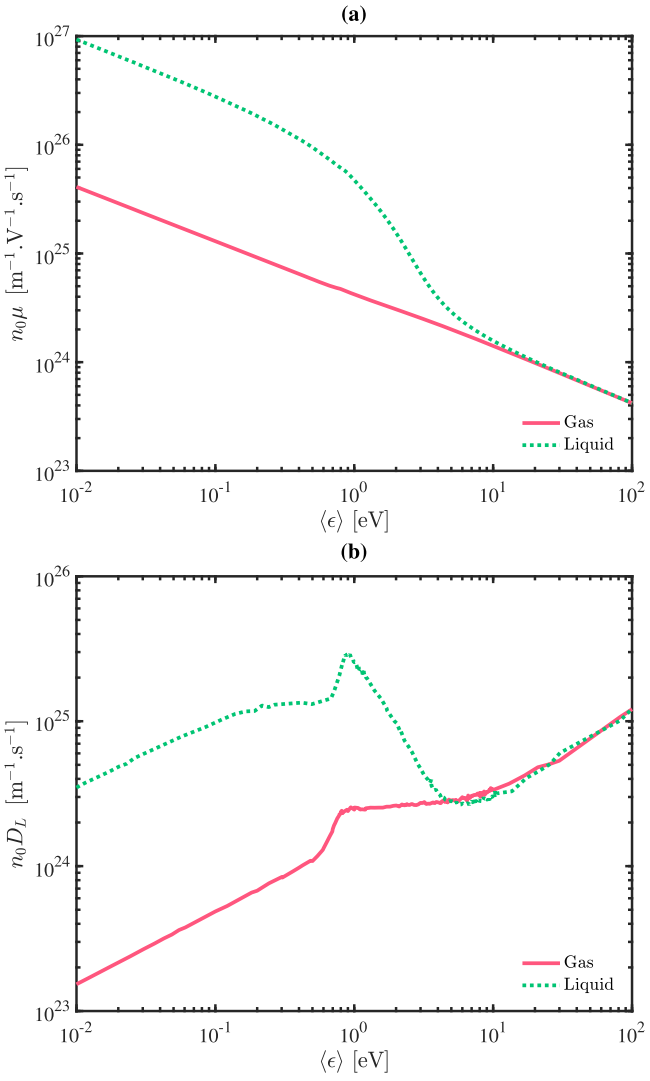

Figure 1. Hydrodynamic transport input data for gas and liquid phase transport for collision model in table 1. (a) Reduced electron mobility coefficient; (b) reduced electron longitudinal diffusion coefficient.

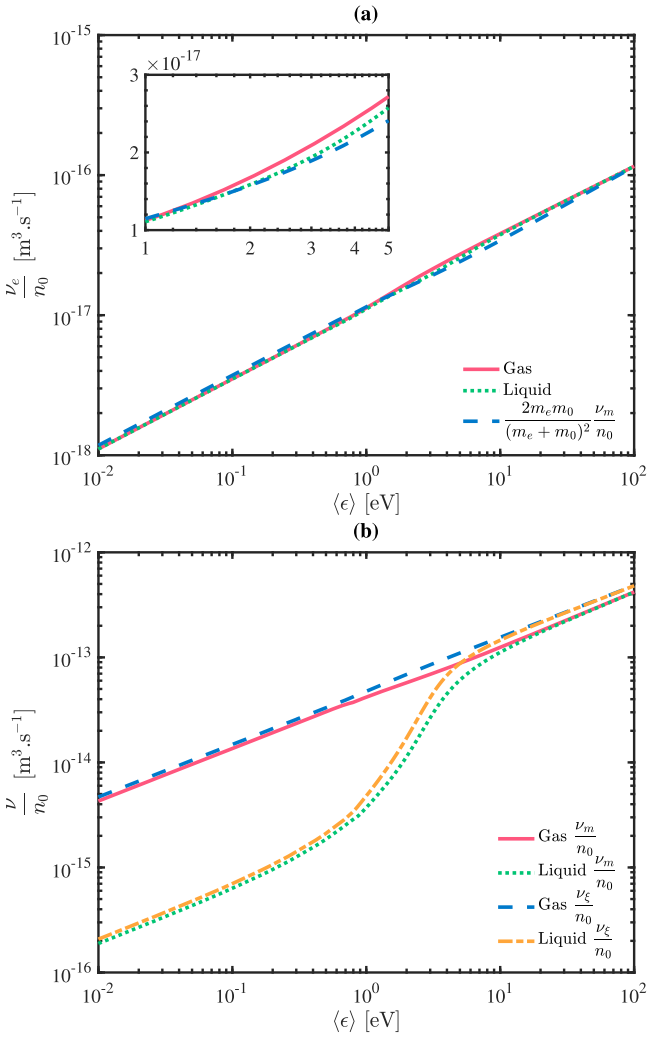

Figure 2. Electron collision rate input data for gas and liquid phase transport for collision model in table 1. (a) Effective reduced energy transfer collision rate, $\frac{\nu_e}{n_0}$; (b) Effective reduced momentum transfer, $\frac{\nu_m}{n_0}$, and energy flux transfer, $\frac{\nu_\xi}{n_0}$, collision rates.

asymptotic convergence of liquid transport to gas phase transport at higher energies.

3.3.2. Collision rates. The reduced collision frequencies of momentum, energy, and energy flux transfer computed from steady state distribution functions are presented in figure 2.

An inset plot in figure 2(a) is included to demonstrate deviation of the curves within an energy range close to the inelastic threshold energy of 2 eV. For comparison we also include a plot of an alternative approach to computing the reduced energy transfer rate [23] often implemented in momentum transfer theory (MTT)

$$\left.\frac{\nu_e}{n_0}\right|_{\text{gas \& liq}} \approx 2\frac{m_e m_0}{(m_e+m_0)^2}\left.\frac{\nu_m}{n_0}\right|_{\text{gas}},$$

to demonstrate the importance of including a specifically computed energy loss rate, S_ϵ^{ss}, and not simply multiplying the gas phase momentum transfer rate by the mass ratio prefactor, often used in MTT collision approximations [12, 37].

The effects of coherent scattering in the liquid phase approximation are clearly evident in figure 2(b), where $\frac{\nu_m}{n_0}$ is multiple orders of magnitude smaller at low energies. As the mean energy of an incoming electron increases, the effects of coherent scattering are reduced and the liquid phase result converges to the gas phase value.

Previously the momentum transfer collision frequency has been used as the collision rate for the energy flux balance equation, owing to the physical similar collisional time scales for the two vector quantities [15, 18]. However, it can be seen in figure 2 that there is a difference between the momentum transfer frequency and a specifically computed energy flux transfer frequency, even in this simple benchmark problem, across both gas and liquid phase media. This supports the claim of using a dedicated energy flux transfer rate as also recommended by Becker and Loffhagen [14, 20].

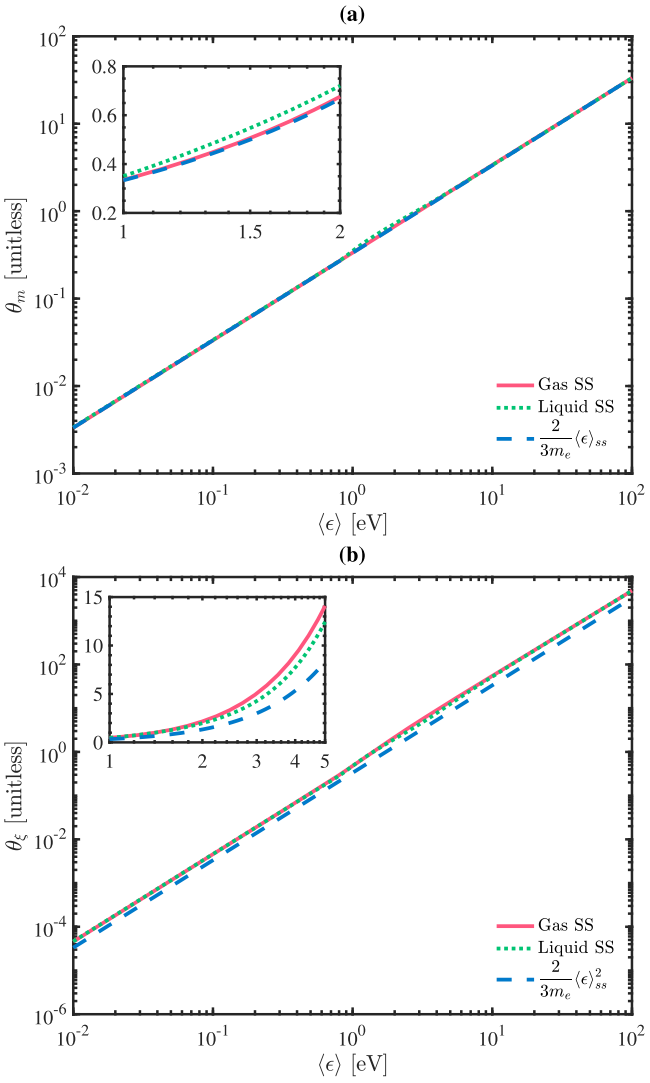

Figure 3. Higher order closure input for gas and liquid media according to collision model in table 1: (a) momentum balance term, θ_m^{ss}; (b) energy flux balance term, θ_ξ^{ss}.

3.3.3. Closure terms. The higher-order moment closure terms θ_m^{ss} and θ_ξ^{ss}, defined by equations (23) and (24) used in the *4MM-SS*/*DDA-SS* models, are plotted against the parameterized moment closure terms, defined by equations (27) and (29) used in the *4MM-D* model, in figure 3.

The inset plots demonstrate there is departure between the approximations once the inelastic channel begins to contribute significantly, specifically on intermediate energy ranges (0.1–10 eV) commonly experienced in non-equilibrium low-temperature plasma modeling. We note a difference between gas and liquid phase values as well, which the parameterized closure does not allow for. This is the primary motivation to preference a direct substitution of steady state data as a function of the electron mean energy, as opposed to parameterizing or assuming a simpler form of the higher order terms.

3.4. Hat field benchmarks

In order to verify against similar benchmarks used in previous works, a simple hat perturbation of a homogeneous background reduced electric field has been adopted [14, 40]. The hat perturbation is placed downstream of an electron source emitting with a constant flux. Fluid models are solved in the steady state over the domain in order to resolve the response of macroscopic variables to the field change. The hat perturbation used previously increases the magnitude of the background reduced electric field with a step function over a defined distance. The geometry of this benchmark is outlined in figure 4.

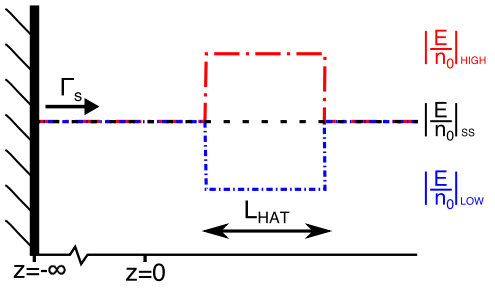

Figure 4. Hat and inverse hat field benchmark problem geometry.

Studying the hat field benchmark allows the effect of inelastic collisions to be studied, and for the performance of fluid models to be evaluated in this field-enhanced collision regime. By increasing the reduced electric field the electron distribution function within the hat samples a larger portion of the inelastic cross-section. If the increased reduced electric field is within a certain range a balance between field driven heating and inelastic cooling is reached. This *window phenomenon* in effect produces oscillating spatial structures in all macroscopic observables [21, 45]. By studying the response of fluid models to this field, we may assess the ability, or inability, of these models to account for such spatial structures.

In addition to the hat field benchmark that increases the magnitude of the reduced electric field, we also simulate an inverse hat field benchmark that reduces the magnitude of the reduced electric field. This inverse hat field model has been chosen in order to examine the relaxation of momentum and energy in low advection problems. Given that closure assumptions of the fluid equations directly impact the divergence of the higher order tensors, and hence the diffusive transport of electron number and energy, we feel it is vital to study a low-field benchmark that emphasizes the impacts of diffusive transport.

We feel that benchmarking against the discussed hat and inverse hat problems provides a suitable breadth of physical conditions to evaluate fluid models presented in this work. For example, the increasing hat field can be compared to potentially sharp gradients found in field-enhanced tip regions of streamer propagation [15, 38] or in sheath regions near boundaries [9, 12]. While conversely, the reduced magnitude of the inverse hat field can be compared to regimes where electric field screening occurs in the channel behind a propagating streamer [15, 38] or where an electric field sheath transitions back into the bulk region of a plasma [9, 12].

3.4.1. Initial and boundary conditions. A source emitting electrons at a constant rate at the background reduced field's steady state mean energy and drift velocity was placed far from the reduced electric field perturbation, such that the electrons had relaxed to a steady-state for the background field before reaching the field step.

Initially the domain was empty, $n(z, 0) = 0$, prior to the source being turned on. Each system of fluid equations was evolved in time, using the numerical method outlined in the appendix, until a steady state solution was reached.

Simple boundary conditions for electron density, and thus fluxes and energy density, are used through fixed Dirichlet conditions

$$n\left(-\frac{L}{2}, t\right) = n\left(\frac{L}{2}, t\right) = 0, \tag{37}$$

where L is the length of the simulation domain. To further reduce the effect of boundaries the computational domain was extended to avoid significant density transport within a fixed distance of the boundaries.

3.4.2. Goodness of fit. In order to quantify how well each fluid model can produce physically accurate results we present a goodness of fit table for each benchmark. Normalized mean square error (NMSE) computations are performed for each fluid model solution when compared to the physically detailed MC solution. The NMSE of an approximation, f_{approx}, compared to an exact value of the function, f_{exact}, is defined as

$$\text{NMSE} = \left\| \frac{f_{\text{exact}} - f_{\text{approx}}}{f_{\text{exact}} - \text{mean}(f_{\text{exact}})} \right\|^2, \tag{38}$$

where $\|...\|$ indicates the 2-norm. In the interpretation of NMSE results, we note the bounds $0 < \text{NMSE} \leqslant \infty$, where $\text{NMSE} = 0$ indicates a perfect fit, $\text{NMSE} = \infty$ indicates a bad fit, and $\text{NMSE} = 1$ implies the approximation is no better a fit than a straight line.

3.4.3. Standard hat field. In figures 5 and 6 we present steady state solutions of each fluid model for the standard hat field benchmark in both gas and liquid phase. Tables 2 and 3 include the NMSE goodness of fit values. For comparison a MC solution of the benchmark problem is included, computed from methods previously used by the JCU group [7, 26]. For the steady state closure method advocated in this work the presented results are the same for both *4MM-SS* and *DDA-SS* models, since the solution is in the steady state.

The fluid model results presented in figures 5 and 6 and NMSE values in tables 2 and 3 demonstrate strong agreement among fluid models for this benchmark in both gas and liquid phases. None of the fluid models can reproduce the periodic structures found in the MC solution, consistent with previous studies [14]. The Fourier and zero heat flux closures offer similar solutions which tend to overshoot on rising and falling edges of the field perturbation. On the other hand, the *4MM-D* and *DDA-SS* solutions are generally monotonic, with the exception of an irregular peak on the falling edge of the hat.

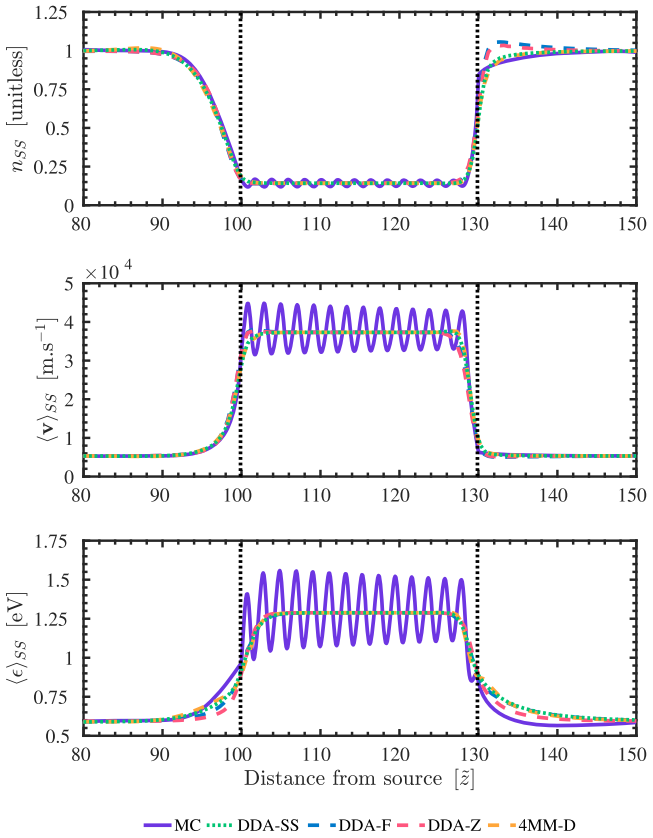

Figure 5. Gas phase hat field perturbation benchmark as per figure 4 where $\tilde{L}_{\text{HAT}} = 30$, $\frac{\mathbf{E}}{n_0} = -1$ Td: -10 Td: -1 Td.

MC simulations demonstrating mean energy heating and cooling either side of the rising and falling edges of the hat are not reproduced to the same magnitude by fluid models. This demonstrates the non-local effects of the electric field change impacting transport properties some distance away. The fluid models appear to be capable of resolving some of this non-local transport but not to the extent found in the MC simulations, particularly in the liquid phase benchmark.

Overall there are minor observable differences among the fluid model results and all NMSE results are very consistent across all variables, approaching zero, indicating a reasonable approximation in the 'line of best fit' sense for all variables with all fluid models used. It can be concluded that using any of the fluid models provides a reasonable approximation to the steady-state electron transport, excluding the periodic electron structures, in cases such as this benchmark.

3.4.4. Inverse hat field. Comparison of the fluid model results in figures 7 and 8 and the NMSE goodness of fit metrics in tables 4 and 5 indicate a significant difference between fluid models in this study. It can be seen the Fourier and zero heat flux models significantly differ to the MC solution, whereas the *4MM-D* and *DDA-SS* models provide a qualitatively closer approximation to the actual solution for number density and mean velocity. The number density profiles for the *DDA-F* and *DDA-Z* models offer a completely different qualitative result compared to the MC result because

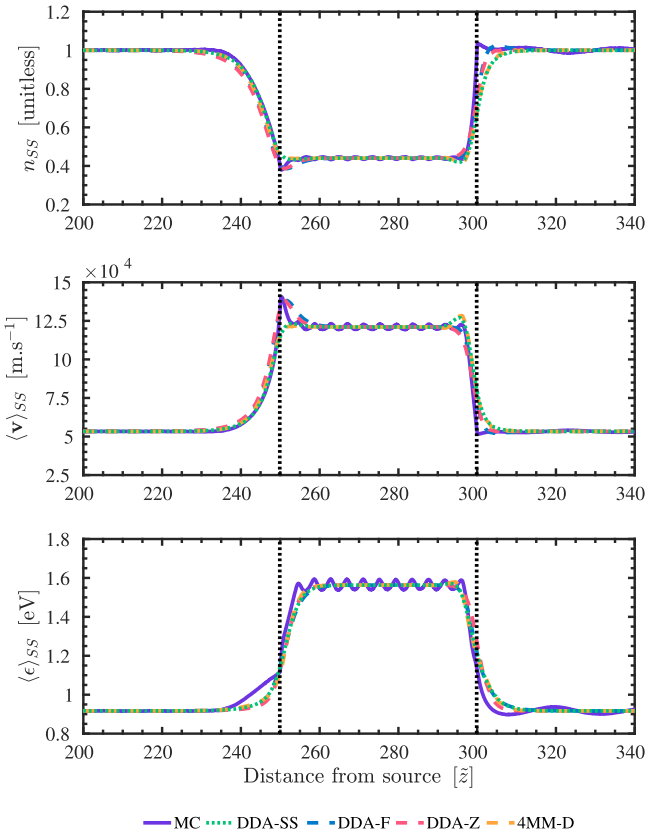

Figure 6. Liquid phase hat field perturbation benchmark as per figure 4 where $\tilde{L}_{\mathrm{HAT}} = 50$, $\frac{\mathbf{E}}{n_0} = -1$ Td: -5 Td: -1 Td.

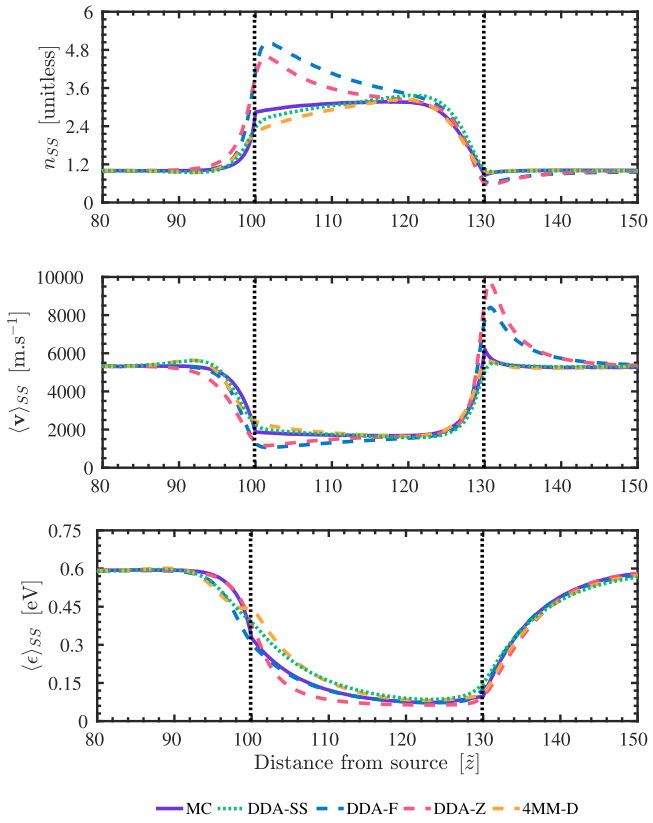

Figure 7. Gas phase inverse hat field perturbation benchmark as per figure 4 where $\tilde{L}_{\mathrm{HAT}} = 30$, $\frac{\mathbf{E}}{n_0} = -1$ Td: -0.1 Td: -1 Td.

Table 2. NMSE for figure 5 solutions for each fluid model compared against Monte Carlo result.

Model	n_{SS}	W_{SS}	$\langle \epsilon \rangle_{\mathrm{SS}}$
DDA-SS	0.004	0.033	0.112
DDA-F	0.010	0.035	0.111
DDA-Z	0.007	0.037	0.111
4MM-D	0.005	0.032	0.112

Table 3. NMSE for figure 6 solutions for each fluid model compared against Monte Carlo result.

Model	n_{SS}	W_{SS}	$\langle \epsilon \rangle_{\mathrm{SS}}$
DDA-SS	0.024	0.016	0.015
DDA-F	0.013	0.011	0.015
DDA-Z	0.015	0.012	0.018
4MM-D	0.022	0.016	0.014

of the overshoot of the mean velocity profiles; in order for the particle flux to remain constant in the steady state, the number density must compensate for the overshoot in the mean velocity, leading to the erroneous results in figures 7 and 8.

The discrepancy between MC results and fluid models is not as pronounced for the liquid phase transport, compared to the gas phase. An effect of the inclusion of coherent scattering for the liquid phase results in a longer momentum relaxation distance in liquid phase transport, which appears to assist the fluid models in reproducing some of the results.

In contrast, the *4MM-D* and *DDA-SS* models provide a better approximation of the mean velocity leading to a closer approximation of the number density, and implying these models handle the low advection transport regime much better than the other two models.

The agreement in the mean energy profiles is much tighter than the lower two moments, with all fluid models doing reasonably well in approximating the MC solution. We note that while *4MM-D* and *DDA-SS* models have very similar NMSE values, figure 7 shows the *4MM-D* model produces incorrect relaxation behavior on the falling edge of the inverse hat. The Fourier model solution offers a very good fit within the hat region, but the inaccuracy of the number density and mean velocity results detracts from this positive result for the *DDA-F* model.

Noticeably, in figure 8, none of the fluid models provide a good approximation to the liquid phase mean energy relaxation inside the inverse hat perturbation. It appears the longer liquid phase relaxation length is better approximated by the *DDA-SS* and *4MM-D* models when compared to the MC mean energy, but the attenuation of the energy is not well described. The opposite appears to be the case for *DDA-F* and *DDA-Z* results, which attenuate the mean energy to a lower value but the relaxation length is considerably different than the MC result.

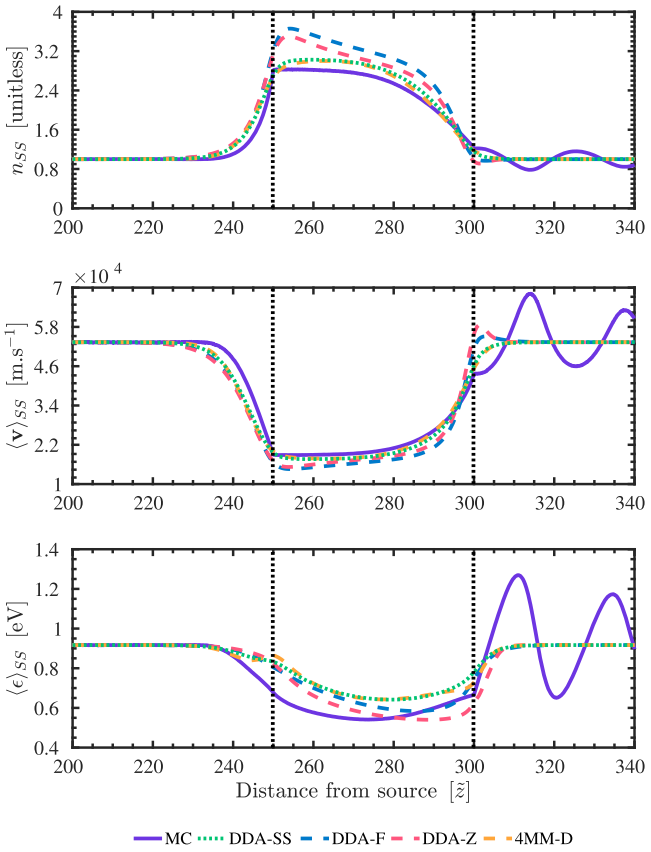

Figure 8. Liquid phase inverse hat field perturbation benchmark as per figure 4 where $\tilde{L}_{\mathrm{HAT}} = 50$, $\frac{\mathbf{E}}{n_0} = -1$ Td: -0.2 Td: -1 Td.

Table 4. NMSE for figure 7 solutions for each fluid model compared against Monte Carlo result.

Model	n_{SS}	W_{SS}	$\langle \epsilon \rangle_{\mathrm{SS}}$
DDA-SS	0.018	0.011	0.017
DDA-F	0.491	0.170	0.008
DDA-Z	0.267	0.293	0.011
4MM-D	0.030	0.014	0.027

Table 5. NMSE for figure 8 solutions for each fluid model compared against Monte Carlo result.

Model	n_{SS}	W_{SS}	$\langle \epsilon \rangle_{\mathrm{SS}}$
DDA-SS	0.037	0.076	0.417
DDA-F	0.228	0.113	0.365
DDA-Z	0.136	0.121	0.361
4MM-D	0.032	0.076	0.421

3.5. Spatiotemporal pulse evolution

As a supplement to the steady state hat field benchmark, which provides some non-equilibrium effects near the field perturbations, the transient evolution of a pulsed Townsend experiment initial pulse was studied to study the ability of the presented fluid models to resolve time-dependent transport effects. Study of this benchmark allows the performance of the fluid models in a sharp gradient, non-hydrodynamic, and non-equilibrium regime to be assessed. For brevity this benchmark is presented for gas phase transport only, as liquid phase results were very similar.

This simulation takes place by releasing the narrow pulse in a homogeneous background reduced field, and simulating the space–time evolution. Sample times were taken at approximately 10 and 100 momentum transfer relaxation times, and five energy transfer relaxation times. These sample times were chosen to demonstrate the solution variations over different physical regimes in order to assess which fluid models provide the best overall response.

For this benchmark comparison a multi-term solution of the Boltzmann equation detailed by Boyle *et al* [27] has been included as a reference solution.

For this benchmark the reduced electric field was fixed at $\frac{\mathbf{E}}{n_0} = -3$ Td such that $W_z = 1.385 \times 10^4$ m s^{-1}, $\langle \epsilon \rangle = 0.8337$ eV are the steady state drift velocity and mean energy respectively.

3.5.1. Initial and boundary conditions. The transient pulse benchmark was set by an initial condition of a narrow Gaussian number density

$$f_n(\tilde{z}) = \frac{1}{\Delta\tilde{z}_0\sqrt{2\pi}} \exp\left[-\frac{1}{2}\left(\frac{\tilde{z}}{\Delta\tilde{z}_0}\right)^2\right], \tag{39}$$

where $\Delta\tilde{z}_0 = 0.1$, and fixed in velocity space by a drifted Maxwellian distribution

$$f_v(\mathbf{v}) = f_n(z)\left(\frac{m}{2\pi k_B T}\right)^{\frac{3}{2}} \exp\left[-\frac{m}{2k_B T}(\mathbf{v} - \mathbf{W})^2\right], \tag{40}$$

where $T = 10^4$ K and $\mathbf{W} = 10^5$ m s^{-1} $\hat{\mathbf{E}}$.

Initial conditions for fluid model computational variables are determined by integrating (15)–(17) over the distribution function

$$f(U, \mathbf{r}, 0) = A f_n(\tilde{z}) f_v(\mathbf{v}), \tag{41}$$

where A is a normalization constant such that $\int U^{\frac{1}{2}} f(U, \mathbf{r}, 0)\mathrm{d}U = 1$. Evaluation of these gives

$$\begin{aligned} n(\mathbf{r}, 0) &= f_n(\tilde{z}) \\ \Gamma(\mathbf{r}, 0) &= f_n(\tilde{z})\mathbf{W}, \\ n_\epsilon(\mathbf{r}, 0) &= f_n(\tilde{z})\left(\frac{3}{2}k_B T + \frac{1}{2}m_e W^2\right), \\ \Gamma_\epsilon(\mathbf{r}, 0) &= f_n(\tilde{z})\left(\frac{5}{2}k_B T + \frac{1}{2}m_e W^2\right)\mathbf{W}. \end{aligned} \tag{42}$$

Dirichlet boundary conditions described for the steady state hat benchmark were employed for the transient pulse evolution.

3.5.2. Number density evolution. The number density evolution displayed in figure 9 demonstrates that at short times dominated by momentum relaxation no fluid model provides an exact replication of the kinetic result, consistent with expected accuracy bounds of fluid models [12, 14, 18].

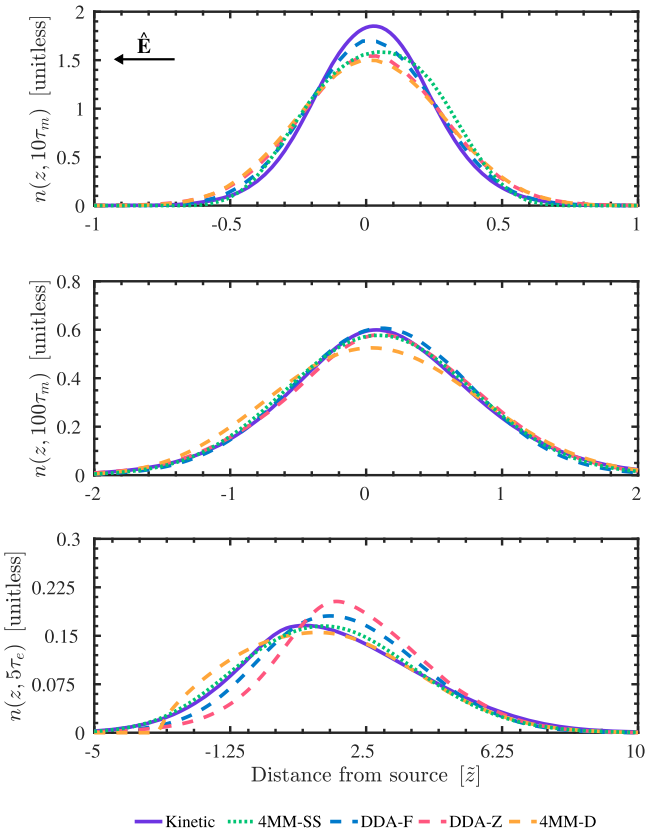

Figure 9. Transient evolution of electron density from narrow Gaussian pulse. Gas phase media as per table 1 with background $\frac{\mathbf{E}}{n_0} = -3$ Td.

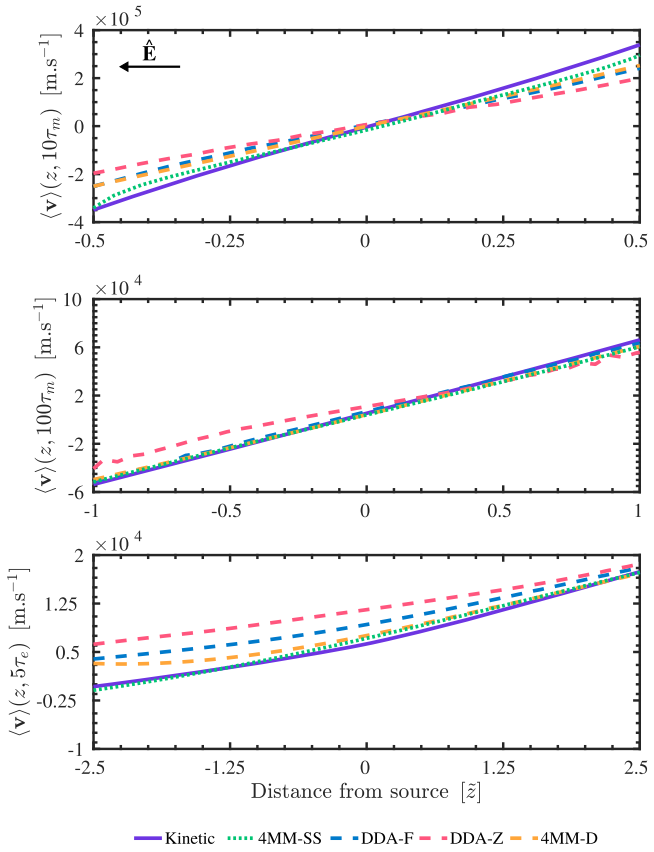

Figure 10. Transient evolution of electron mean velocity from narrow Gaussian pulse. Gas phase media as per table 1 with background $\frac{\mathbf{E}}{n_0} = -3$ Td.

Despite all fluid model results being more diffusive than the kinetic solution, none demonstrate concerning variation from the general qualitative behavior of the accurate kinetic solution.

Considering the intermediate regime between momentum and energy relaxation processes in figure 9 shows better agreement to the kinetic solution for all fluid models apart from the *4MM-D* model. This demonstrates the effects of higher density diffusivity due to closure assumptions in the *4MM-D* model.

As time continues, and energy relaxation becomes the dominant process, the variation between fluid solutions is shown in figure 9. It can be plainly seen the zero heat flux and Fourier closure assumptions produce profiles that poorly fit the kinetic result. They are both forward peaked, and inaccurately predict the back-diffusion seen behind the bulk of the pulse. The *4MM-D* closure performs slightly better, except in the region behind the bulk of the pulse, where it appears back-diffusion has not been modeled accurately. Finally we see the *4MM-SS* result remains a suitable 'line of best fit' approximation to the kinetic solution.

3.5.3. Mean velocity evolution. From the evolution of mean velocity shown in figure 10 it can be seen that the *4MM-SS* continues to provide a closer approximation to the kinetic solution across all three time scales. At early times, the non-hydrodynamic transport of the kinetic solution is not replicated by any fluid model yet the steady state closure provides the closest comparison compared to the other discussed fluid models.

During the transition between momentum and energy relaxation times there is better comparison for most of the fluid models, with the exception of the zero heat flux model. However at the longest time scale the discrepancies between each fluid model can be seen. In the regions close to, and behind, the origin the mean velocity is best predicted by the *4MM-SS* model. While the remaining fluid models provide an over estimation of the mean velocity, particularly in back diffusion regions behind the origin. As the pulse relaxes into a smooth-gradient hydrodynamic regime, the agreement becomes asymptotically better across all fluid models, as one might expect.

3.5.4. Mean energy evolution. Mean energy variation is much simpler to identify in this benchmark compared to the previous macroscopic observables. At short times figure 11 shows a qualitative agreement to the quadratic-like shape of the kinetic solution—apart from the *4MM-D* model. The zero heat flux model underestimates the mean energy consistently, while the Fourier closure appears to perform quite well. The *4MM-SS* model overestimates the mean energy in the bulk of the pulse, and underestimates on the fringes. Overall, the

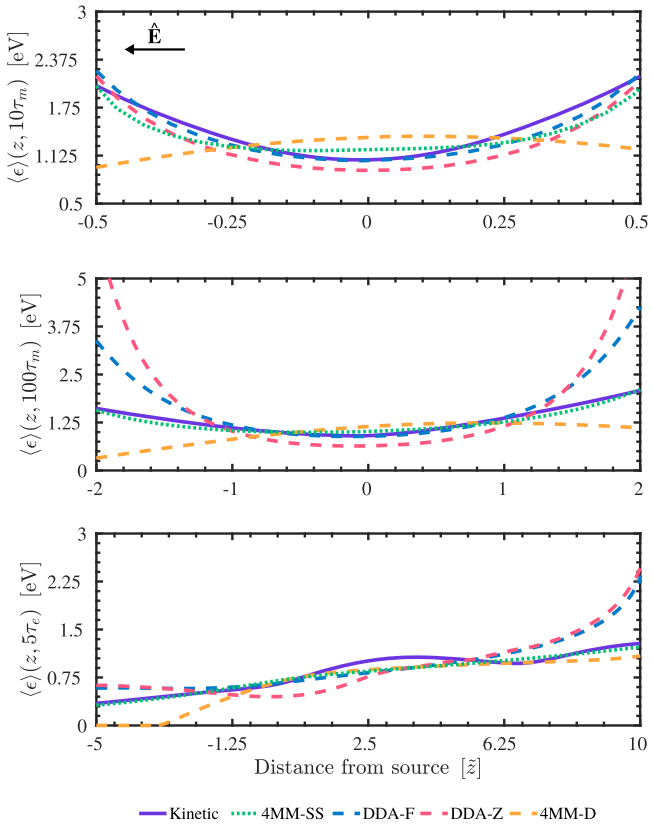

Figure 11. Transient evolution of electron mean energy from narrow Gaussian pulse. Gas phase media as per table 1 with background $\frac{\mathbf{E}}{n_0} = -3$ Td.

approximations of most fluid models perform qualitatively well in this time sample.

As time advances into the two final sample times in figure 11, it can be seen most fluid models fail to approximate the kinetic solution well apart from the *4MM-SS* model. The *DDA-Z* and *DDA-F* models show that on the fringes of the pulse the mean energy is severely overestimated, while generally underestimating in the bulk of the pulse. The *4MM-D* model continues to suffer inaccuracies in regions experiencing back diffusion effects, but does regain some accuracy in the long time regime when predicting the energy relaxation into the hydrodynamic regime.

The *4MM-SS* demonstrates the ability to generally resolve a 'line of best fit' approximation to the kinetic solution across multiple time scales. As a supplementary benchmark to the steady state hat field benchmark results, we believe the presented transient evolution results are a good indicator of the general accuracy that the *4MM-SS* steady state distribution closure provides. We believe the strength of this model lies in reverting to a steady state limit to provide a physical distribution when predicting transport, this is especially clear in regions where back diffusion of energy and density are found.

3.6. Distribution effects and implications for fluid modeling

In order to understand the results and limitations of the presented fluid models the energy distribution function was studied. Given that the majority of modern fluid models

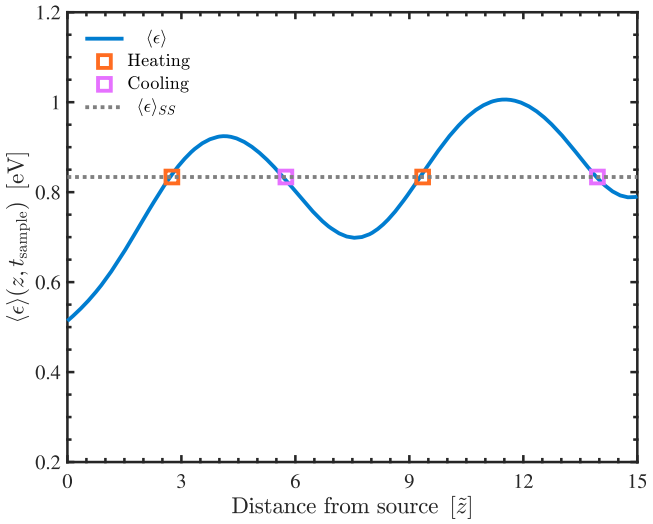

Figure 12. Transient mean energy evolution at $t_{\text{sample}} \approx 5\tau_e$ indicating sample points coinciding with $\langle\epsilon\rangle_{\text{ss}} = 0.8337$ eV.

utilize the local mean energy approximation in evaluation of collisions, and possibly closure, it is important to understand the role of the distribution function in producing results such as spatially periodic structures that fluid models currently cannot reliably produce.

In order to study the energy distribution function effects a transient kinetic solution of the Boltzmann equation, discussed in the previous section, was sampled after approximately five energy relaxation time periods, $5\tau_e$. At this time the initial energy distribution will have sufficiently relaxed to reduce sharp non-hydrodynamic effects. At the sample time the mean electron energy can be plotted, as shown in figure 12, and samples in position-space can be taken where the mean-energy coincides with the steady-state mean energy value of 0.8337 eV.

The typical form of the distribution function component $U^{\frac{1}{2}} f_0(U)$ at the spatial points corresponding to the same steady-state mean energy value are shown in figure 13. For comparison the steady-state energy distribution function component, found by simulating the kinetic solution for a very long time, and that of a drifted Maxwellian energy distribution function, coinciding with the steady-state drift and energy, are also plotted.

From the representative distribution functions it can be seen the qualitative form of the energy distribution function varies significantly between heating and cooling regimes in the transient evolution. It was found that distribution functions on the leading edge of a so called Franck–Hertz oscillation correspond to a forward peaked distribution function, but do not significantly impinge past the inelastic threshold until they reach the peak of the oscillation. Conversely, samples on the falling edge of the oscillation contain a bimodal distribution due to inelastic collisions shifting high energy electrons that were gradually heated on the leading edge regime down to a lower energy in the distribution.

Compared to the steady-state and drifted Maxwellian distribution function both heating and cooling distributions are quite different. As a result we determine that this

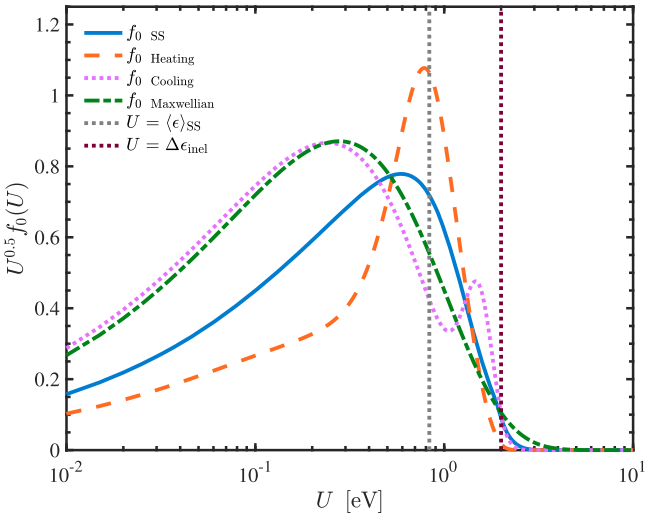

Figure 13. Comparison of typical energy distribution functions, $U^{\frac{1}{2}} f_0(U)$, for transient heating and cooling regimes. Steady state distribution and drifted Maxwellian shown for comparison.

distribution variation is a key cause of the deficiencies in the local mean energy approximation used in plasma fluid modeling. Until the local mean energy approximation is improved, in order to capture distribution variation, the complex spatial structures such as Franck–Hertz oscillations, will not be resolvable with a fluid method.

4. Conclusion

In this study we have presented the framework for a unified approach to electron fluid modeling in gas or liquid media. Through coherent scattering modifications, the fluid model accommodates some liquid structure effects which have a considerable effect on electron transport. Furthermore, the model has the flexibility of incorporating future additional liquid processes, such as solvation, via including additional electron collision cross sections into the computation of steady state collision rates.

Within the presented fluid model framework, we have implemented a fluid equation closure method that we believe has the ability to consistently produce physically sound approximations across a wide range of regimes in both gas and simple liquid media. Comparison to fluid models commonly used in the low-temperature plasma modeling community was performed, and demonstrated improvements were observed in low field regimes. This was demonstrated by a series of high electric field and low electric field hat benchmarks, solved for analogous gas and liquid phase electron transport with a simplified step-inelastic collision model. Despite the simplicity of the collision model, and the benchmarks, we believe the results presented emphasize the importance of closure in fluid modeling, and the ability of the steady state closure method to obtain good approximations across different physical regimes.

To supplement the steady state hat field benchmarks, the impacts of closure on the transport of a transient non-hydrodynamic, non-equilibrium pulse in a homogeneous reduced electric field were also presented. It was shown that over multiple time scales, the approximation of an accurate multi-term Boltzmann equation solution was best estimated by the steady state closure assumption.

Finally, we addressed an energy distribution effect that we believe contributes significantly to the inability of fluid models to reproduce spatial periodic structures, such as Franck–Hertz oscillations. It was shown that although generally sound, in a spatially averaged sense, the local mean energy approximation of collision, and closure, terms will not be able to reproduce strongly varying distribution function effects in its current form. Field driven heating and inelastic collision driven cooling regimes were shown to produce widely different distribution functions in a periodic structure regime, which the LEA simply cannot produce in its current form.

In this work we have laid the foundation for applying the presented electron fluid model to the study of electron transport in simulated plasma–liquid interfaces in future work. We hope to motivate future additions of other liquid effects into fluid modeling, such as polar liquid effects and electron solvation processes. We also look to stimulate further studies on improving collision approximation methods in order to capture distribution effects, and novel methods of closing higher order moments in charged particle fluid modeling.

Acknowledgments

NG acknowledges financial support from the Australian Government through the Australian Postgraduate Award, and JCU through the HDR Research Enhancement Scheme. SD acknowledges support from MPNTRRS Projects OI171037 and III41011.

Appendix. Numerical considerations

A.1. Solution scheme

The systems of hyperbolic transport equations were solved using a finite differences FCT method [42–44]. Using the FCT method a monotonic, stable lower order solution was implemented via first order upwinding on vector divergences and second order central differences on scalar gradients [43, 44]. This lower order scheme was enhanced by a fourth order central difference scheme as prescribed by Zalesak [43]. As for the fourth order discretization, the FCT flux limiter prescribed by Zalesak was used in this work.

Time stepping was performed via the Runge–Kutta fourth order method with a Courant–Friedrich–Lewy (CFL) condition imposed to ensure stability. The CFL condition was fixed to ensure Δt did not exceed reasonable fractions of momentum and energy relaxation time scales. Overall the solution scheme generally provides fourth order accuracy in time and space, however to ensure physical solutions, it may

reduce to a nonlinear combination of the first and fourth order schemes in the presence of sharp gradients [44].

Benchmarking of the numerical scheme was performed on simpler test problems before applying to more involved models discussed in this work. The numerical scheme was successfully benchmarked against square-wave advection problems, Gaussian pulse advection-diffusion problems, and Sod's shock tube benchmark CFD problem [42–44].

A.2. Dimensional scaling

Before numerically solving the systems of equations presented dimensional scaling was performed. Scaling is done in order to introduce numerically sound quantities on the order of unity, for example converting Joules to electronvolts. Additionally, this allows neutral gas density dependence to be scaled out of the systems of equations, by introducing variables such as the reduced electric field, $\frac{\mathbf{E}}{n_0}$.

The length scale of this study is a scattering mean free path, $\tilde{\lambda}$, in a neutral gas of density n_0 with a representative scattering cross section of $\sigma_0 = 1$ Å^2

$$\tilde{\lambda} = \frac{1}{\sigma_0 n_0} \text{ m},$$

such that $z = \tilde{\lambda}\tilde{z}$ where $\tilde{z}$ is a dimensionless length variable.

The electron mass is simply chosen as the mass unit scale such that conversion from dimensionless mass $\tilde{m}$ is

$$m = m_e \tilde{m}.$$

While an energy of 1 eV is simply chosen as the energy unit scale so that such that conversion from electronvolts $\tilde{\epsilon}$ is

$$\epsilon = e\tilde{\epsilon}.$$

A time scale can be defined via the chosen mass, length, and energy scales

$$\tilde{\tau} = \tilde{\lambda}\sqrt{\frac{m_e}{2e}} \text{ s},$$

such that $t = \tilde{\tau}\tilde{t}$ where $\tilde{t}$ is dimensionless time.

Finally, the reduced electric field of $1\,\text{Td} = 1 \times 10^{-21}\,\text{Vm}^2$ is chosen as the field scale,

$$\frac{\mathbf{E}}{n_0} = 1 \times 10^{-21}\frac{\tilde{\mathbf{E}}}{n_0} \text{ Vm}^2,$$

where $\frac{\tilde{\mathbf{E}}}{n_0}$ is the reduced field in Townsend.

A.3. Hat field benchmark numerics

Discretization of the hat field benchmark was fixed by a fraction of the Franck–Hertz wavelength of any expected periodic structures that are known to appear for this collision model [45, 47]. The Franck–Hertz wavelength for a given collision model is

$$\tilde{\lambda}_{\text{FH}} = \frac{\epsilon_{\text{inel}}}{0.1\frac{E}{n_0}},$$

where ϵ_{inel} is the threshold energy of the inelastic process in eV and $\frac{E}{n_0}$ is the reduced electric field in Townsend [47]. In this work the spatial step size was fixed at $\Delta\tilde{z} = \frac{\tilde{\lambda}_{\text{FH}}}{40}$ with a CFL condition of $\frac{\Delta\tilde{t}}{\Delta\tilde{z}} = 0.1$ imposed.

A.4. Transient pulse benchmark numerics

Numerical discretization of the fluid model solutions was forced to be the same as the detailed kinetic solution used to compare performance of the models. The details and implementation of the kinetic solution used as a benchmark solution in this study can be found in the recent work of Boyle *et al* [27]. The consistent discretization scheme was chosen to give a stronger basis for comparing solutions directly.

ORCID

D G Cocks https://orcid.org/0000-0002-9943-7100

References

[1] Bruggeman P J *et al* 2016 Plasma–liquid interactions: a review and roadmap *Plasma Sources Sci. Technol.* **25** 053002
[2] Babaeva N Y, Tian W and Kushner M J 2014 The interaction between plasma filaments in dielectric barrier discharges and liquid covered wounds: electric fields delivered to model platelets and cells *J. Phys. D: Appl. Phys.* **47** 235201
[3] Lietz A M and Kushner M J 2016 Air plasma treatment of liquid covered tissue: long timescale chemistry *J. Phys. D: Appl. Phys.* **49** 425204
[4] Robson R E and Ness K F 1986 Velocity distribution function and transport coefficients of electron swarms in gases: spherical-harmonics decomposition of Boltzmann's equation *Phys. Rev.* A **33** 2068–77
[5] Ness K F and Robson R E 1986 Velocity distribution function and transport coefficients of electron swaiiiis in gases: II. Moment equations and applications *Phys. Rev.* A **34** 2185
[6] Hagelaar G J M and Pitchford L C 2005 Solving the Boltzmann equation to obtain electron transport coefficients and rate coefficients for fluid models *Plasma Sources Sci. Technol.* **14** 722–33
[7] Dujko S, White R D and Petrovic Z L 2008 Monte Carlo studies of non-conservative electron transport in the steady-state Townsend experiment *J. Phys. D: Appl. Phys.* **41** 245205
[8] White R D, Robson R E, Dujko S, Nicoletopoulos P and Li B 2009 Recent advances in the application of Boltzmann equation and fluid equation methods to charged particle transport in non-equilibrium plasmas *J. Phys. D: Appl. Phys.* **42** 194001
[9] Boeuf J P and Pitchford L C 1995 Two-dimensional model of a capacitively coupled rf discharge and comparisons with experiments in the gaseous electronics conference reference reactor *Phys. Rev.* E **51** 1376–90
[10] Hagelaar G J M and Kroesen G M W 2000 Speeding up fluid models for gas discharges by implicit treatment of the electron energy source term *J. Comput. Phys.* **159** 1–12
[11] Kushner M J 2004 Modeling of microdischarge devices: pyramidal structures *J. Appl. Phys.* **95** 846
[12] Robson R E, White R D and Petrović Z L 2005 Colloquium: physically based fluid modeling of collisionally dominated low-temperature plasmas *Rev. Mod. Phys.* **77** 1303–20

[13] van Dijk J, Peerenboom K, Jimenez M, Mihailova D and van der Mullen J 2009 The plasma modelling toolkit Plasimo *J. Phys. D: Appl. Phys.* **42** 194012
[14] Becker M M and Loffhagen D 2013 Enhanced reliability of drift-diffusion approximation for electrons in fluid models for nonthermal plasmas *AIP Adv.* **3** 012108
[15] Markosyan A H, Teunissen J, Dujko S and Ebert U 2015 Comparing plasma fluid models of different order for 1D streamer ionization fronts *Plasma Sources Sci. Technol.* **24** 065002
[16] Becker M M, Kählert H, Sun A, Bonitz M and Loffhagen D 2017 Advanced fluid modeling and PIC/MCC simulations of low-pressure ccrf discharges *Plasma Sources Sci. Technol.* **26** 44001
[17] Boeuf J P 1987 Numerical model of rf glow discharges *Phys. Rev.* A **36** 2782–92
[18] Dujko S, Markosyan A H, White R D and Ebert U 2013 High-order fluid model for streamer discharges: I. Derivation of model and transport data *J. Phys. D: Appl. Phys.* **46** 475202
[19] Tsendin L D 2010 Nonlocal electron kinetics in gas-discharge plasma *Phys.—Usp.* **53** 133–57
[20] Becker M M and Loffhagen D 2013 Derivation of moment equations for the theoretical description of electrons in nonthermal plasmas *Adv. Pure Math.* **03** 343–52
[21] Nicoletopoulos P and Robson R E 2008 Periodic electron structures in gases: a fluid model of the 'window' phenomenon *Phys. Rev. Lett.* **100** 1–4
[22] Nicoletopoulos P, Robson R E and White R D 2012 Fluid-model analysis of electron swarms in a space-varying field: nonlocality and resonance phenomena *Phys. Rev.* E **85** 1–7
[23] White R D and Robson R E 2011 Multiterm solution of a generalized Boltzmann kinetic equation for electron and positron transport in structured and soft condensed matter *Phys. Rev.* E **84** 1–10
[24] Tian W and Kushner M J 2014 Atmospheric pressure dielectric barrier discharges interacting with liquid covered tissue *J. Phys. D: Appl. Phys.* **47** 165201
[25] Gopalakrishnan R, Kawamura E, Lichtenberg A J, Lieberman M A and Graves D B 2016 Solvated electrons at the atmospheric pressure plasma-water anodic interface *J. Phys. D: Appl. Phys.* **49** 295205
[26] Tattersall W J, Cocks D G, Boyle G J, Buckman S J and White R D 2015 Monte Carlo study of coherent scattering effects of low-energy charged particle transport in Percus–Yevick liquids *Phys. Rev.* E **91** 43304
[27] Boyle G J, Tattersall W J, Cocks D G, McEachran R P and White R D 2017 A multi-term solution of the space–time Boltzmann equation for electrons in gases and liquids *Plasma Sources Sci. Technol.* **26** 24007
[28] Cohen M and Lekner J 1967 Theory of hot electrons in gases, liquids, and solids *Phys. Rev.* **158** 305–9
[29] Sakai Y 2007 Quasifree electron transport under electric field in nonpolar simple-structured condensed matters *J. Phys. D: Appl. Phys.* **40** R441–52
[30] Dujko S, White R D, Petrovic Z L and Robson R E 2011 A multi-term solution of the nonconservative Boltzmann equation for the analysis of temporal and spatial non-local effects in charged-particle swarms in electric and magnetic fields *Plasma Sources Sci. Technol.* **20** 024013
[31] Robson R E, Nicoletopoulos P, Hildebrandt M and White R D 2012 Fundamental issues in fluid modeling: direct substitution and aliasing methods *J. Chem. Phys.* **137** 214112
[32] Turner M M, Derzsi A, Donkó Z, Eremin D, Kelly S J, Lafleur T and Mussenbrock T 2013 Simulation benchmarks for low-pressure plasmas: capacitive discharges *Phys. Plasmas* **20** 013507
[33] Wang-Chang C S, Uhlenbeck G E and deBoer J 1964 The heat conductivity and viscosity of polyatomic gases *Studies in Statistical Mechanics* vol II (New York: Wiley) p 241
[34] van Hove L 1954 Correlations in space and time and Born approximation in systems of interacting particles *Phys. Rev.* **95** 249
[35] Becker M M and Loffhagen D 2013 Consistent description of electron transport in fluid models for nonthermal plasmas *ICPIG XXXI* pp 2–5
[36] Sigeneger F and Loffhagen D 2016 Fluid model of a single striated filament in an RF plasma jet at atmospheric pressure *Plasma Sources Sci. Technol.* **25** 035020
[37] Robson R E 2006 *Introductory Transport Theory for Charged Particles in Gases* (Singapore: World Scientific)
[38] Dujko S, Markosyan A H and Ebert U 2013 High-order fluid model for streamer discharges: II. Numerical solution and investigation of planar fronts *J. Phys. D: Appl. Phys.* **47** 475203
[39] Ramamurthi B, Economou D J and Kaganovich I D 2003 Effect of non-local electron conductivity on power absorption and plasma density profiles in low pressure inductively coupled discharges *Plasma Sources Sci. Technol.* **12** 170–81
[40] Sigeneger F and Winkler R 1999 Nonlocal transport and dissipation properties of electrons in inhomogeneous plasmas *IEEE Trans. Plasma Sci.* **27** 1254–61
[41] Bittencourt J A 2004 *Fundamentals of Plasma Physics* (New York: Springer)
[42] Boris J P 1973 Flux corrected transport *J. Comput. Phys.* **11** 38–69
[43] Zalesak S T 1979 Fully multidimensional algorithms naval research flux-corrected for fluids *J. Comput. Phys.* **31** 335–62
[44] Kuzmin D, Lohner R and Turek S 2005 Flux-corrected transport: principles, algorithms, and applications *Scientific Computation* (Berlin: Springer)
[45] Robson R E E, Li B and White R D D 2000 Spatially periodic structures in electron swarms and the Franck–Hertz experiment *J. Phys. B: At. Mol. Opt. Phys.* **33** 507–20
[46] Verlet L and Weis J-J 1972 Equilibrium theory of simple liquids *Phys. Rev.* A **5** 939
[47] White R D, Robson R E, Nicoletopoulos P and Dujko S 2012 Periodic structures in the Franck–Hertz experiment with neon: Boltzmann equation and Monte-Carlo analysis *Eur. Phys. J.* D **66** 1–9